

Tailoring the Lithium Deposition on Cu Substrate by a Functionalized-Polysiloxane Layer

Rio Akbar Yuwono,^[a] Peng-Xuan Yu,^[a] Ruben Foeng,^[a] Chusnul Khotimah,^[a] Salva Salshabilla,^[a] Fu-Ming Wang,^{*[a, b, c, d]} Mao-Tsu Tang,^[e] and Nae-Lih Wu^[f, g]

Owing to the high theoretical capacity of 3860 mAh g⁻¹ and low redox potential, lithium metal is the best candidate for the development of next generation high-energy density lithium-ion batteries. However, notorious lithium dendrites growth and the poor compatibility of liquid electrolyte hinder the commercialization of lithium metal batteries. In this work, an anode-less system was used to understand the change in lithium deposition on Cu current collector after the additional functionalized-polysiloxane (PE) layer. The PE structure consists of lithiophobic and lithiophilic side chains which facilitate the

uniform lithium deposition on Cu substrate. This evidence was collected by scanning electron microscopy (SEM) after the cycling test of half-cell configuration and the lithium deposition with different current densities. The reversibility was improved by 5% compared with the bare Cu. In addition, the potential polarization was lowered after the addition of PE layer on bare Cu. Thus, the higher cycle stability (40%) and more stable coulombic efficiency are observed on the PE@Cu || NCM83 cell compared with the bare-Cu || NCM83 during the cycle test.

Introduction

Lithium-ion batteries (LIBs) are believed to be one of keys to reducing the carbon footprint; especially to power electric vehicles (EVs). In China, EVs would account for 35% of the total number of vehicles in 2030.^[1] This stipulates the need for the development of high energy density LIBs to reduce anxiety while driving the EVs due to it taking too long to refill compared to internal combustion engine. Moreover, most

countries still do not have an enough charging infrastructure for the EVs.^[2] To overcome this challenge, development is necessary to be made on the LIBs components. One of the keys to improving the high energy density is by using high-capacity cathode (e.g., layered Ni-rich oxide) and or high-capacity anode material (e.g., Li metal). The cathode determines the amount of Li that can be utilized, meanwhile the high-capacity anode reduces the overall weight of the battery. Li metal is one of the superior candidates of anode material for high energy density LIBs due to a high theoretical capacity of 3860 mAh g⁻¹ and a low redox potential of -3.04 V versus standard hydrogen electrode (SHE). However, the high reactivity and the high energy contents of Li metal raise the safety concerns of the battery.^[3,4]

To reduce the safety concerns of using Li metal, the amount of Li metal has to be kept as low as possible. Moreover, an excess of Li metal decreases the theoretical volumetric capacity of the battery.^[5] A battery with an excess Li metal of 200% exhibits a lower volumetric capacity than used a graphite anode.^[6] This born to concept of anode-free or zero-excess lithium metal batteries (AFLMB or ZELMB). In which only current collector, commonly cooper, as the negative electrode.^[7] Thus, an N/P ratio of 0 is expected. However, the low affinity to lithium results in the nonuniform lithium plating on Cu substrate. This easily induces the formation of lithium dendrites as well as dead lithium.^[8,9] Therefore, the battery suffers from poor reversibility when it combines with cathode, where the lithium inventory is limited. Then, a small amount of lithium is initially deposited on Cu to compensate for this poor reversibility in the first cycle.^[10-12] In which the term of anode-less is way more suitable than anode-free or zero-excess lithium.^[12] But still this concept improves the safety of the battery and reduces the handling difficulty compared to using Li metal. For that reason, this system is suitable to study the lithium deposition, lithium dendrite growth, and the reactivity between

[a] R. Akbar Yuwono, P.-X. Yu, R. Foeng, C. Khotimah, S. Salshabilla, F.-M. Wang
Graduate Institute of Applied Science and Technology, National Taiwan University of Science and Technology, No.4, Keelung Rd., Sec.4, Da'an District, Taipei City 106335, Taiwan R.O.C.
E-mail: mccabe@mail.ntust.edu.tw

[b] F.-M. Wang
Graduate Institute of Energy and Sustainability Technology, National Taiwan University of Science and Technology, No.4, Keelung Rd., Sec.4, Da'an District, Taipei City 106335, Taiwan R.O.C.

[c] F.-M. Wang
Department of Chemical Engineering, Chung Yuan Christian University, No. 200, Chung Pei Rd., Zhongli District, Taoyuan City 320314, Taiwan R.O.C.

[d] F.-M. Wang
R&D Center for Membrane Technology, Chung Yuan Christian University, No. 493, Xinzhong N. Rd., Zhongli District, Taoyuan City 320314, Taiwan R.O.C.

[e] M.-T. Tang
National Synchrotron Radiation Research Center, No. 101, Hsin-Ann Rd., Hsinchu Science Park, Hsinchu City 300092, Taiwan R.O.C.

[f] N.-L. Wu
Department of Chemical Engineering, National Taiwan University, No.1, Sec.4, Roosevelt Rd., Da'an District, Taipei City 10617, Taiwan R.O.C.

[g] N.-L. Wu
Advanced Research Center for Green Materials Science and Technology, National Taiwan University, No.1, Sec.4, Roosevelt Rd., Da'an District, Taipei City 10617, Taiwan R.O.C.

 Supporting information for this article is available on the WWW under <https://doi.org/10.1002/batt.202400488>

lithium and electrolyte for the sake of low-excess Li metal batteries development.^[10,13–19]

Herein, a functionalized polysiloxane (PE) layer is developed to understand its influence on the lithium deposition in anodeless system with carbonate-based electrolyte. The ether-based is known for having a better stability towards near zero potential than carbonate-based electrolyte.^[20] In addition, it avoids the dendritic-like of the deposited lithium on Cu substrate.^[17] However, the ether-based has lower oxidation (4.0 V vs. Li/Li⁺) potential than carbonate-based electrolytes (> 4.0 V vs. Li/Li⁺).^[21,22] this limits the cathode selectivity if using ether-based. Thus, the use of carbonate-based solvent allows the utilization of the high energy density cathode material; such layered Ni-rich oxide cathode.^[18]

Poly(methylhydrosiloxane) (PMHS), poly(ethyl glycol) methyl ether methacrylate (PEGMEMA), and 2-carboxyethyl acrylate (CEA) mixture are synthesized through a Pt catalyzed hydro-silylation reaction to produce PE with an additional Li source from lithium hydroxide. PMHS is utilized as a lithiophobic chains, while PEGMEMA is purposed as a lithiophilic side chains

as well as to prevent the lithium dendrites growth in lower potential,^[23] and CEA as a lithium carrier to increase the affinity to lithium along with the compensation of the poor reversibility.^[24] The strategy is to utilize the lithiophobic and lithiophilic side chains of PE that facilitate the unique lithium migration pathway^[25–27], which helps to prevent the random lithium deposition on Cu substrate. This is then improving the cycle stability of the full cell configuration with LiNi_{0.83}Co_{0.12}Mn_{0.05}O₂ (NCM83) as a cathode.

Results and Discussion

The proton NMR of precursors and the synthesized product are shown in Figure 1a–e. The CH₃ and Si–H functional groups of PMHS are denoted in "a" and "b" (Figure 1a). Peak "a" and "b" are positioned at 0.12 ppm and 0.47 ppm, respectively. The calculated integral ratio of peak "a" over peak "b" is 0.31. The PEGMEMA exhibits ¹H-NMR at δ (ppm) of 5.48–6.02 (peak "g"), 4.2 (peak "e"), 3.54 (peak "d"), 3.27 (peak "c"), and 1.84 (peak "f")

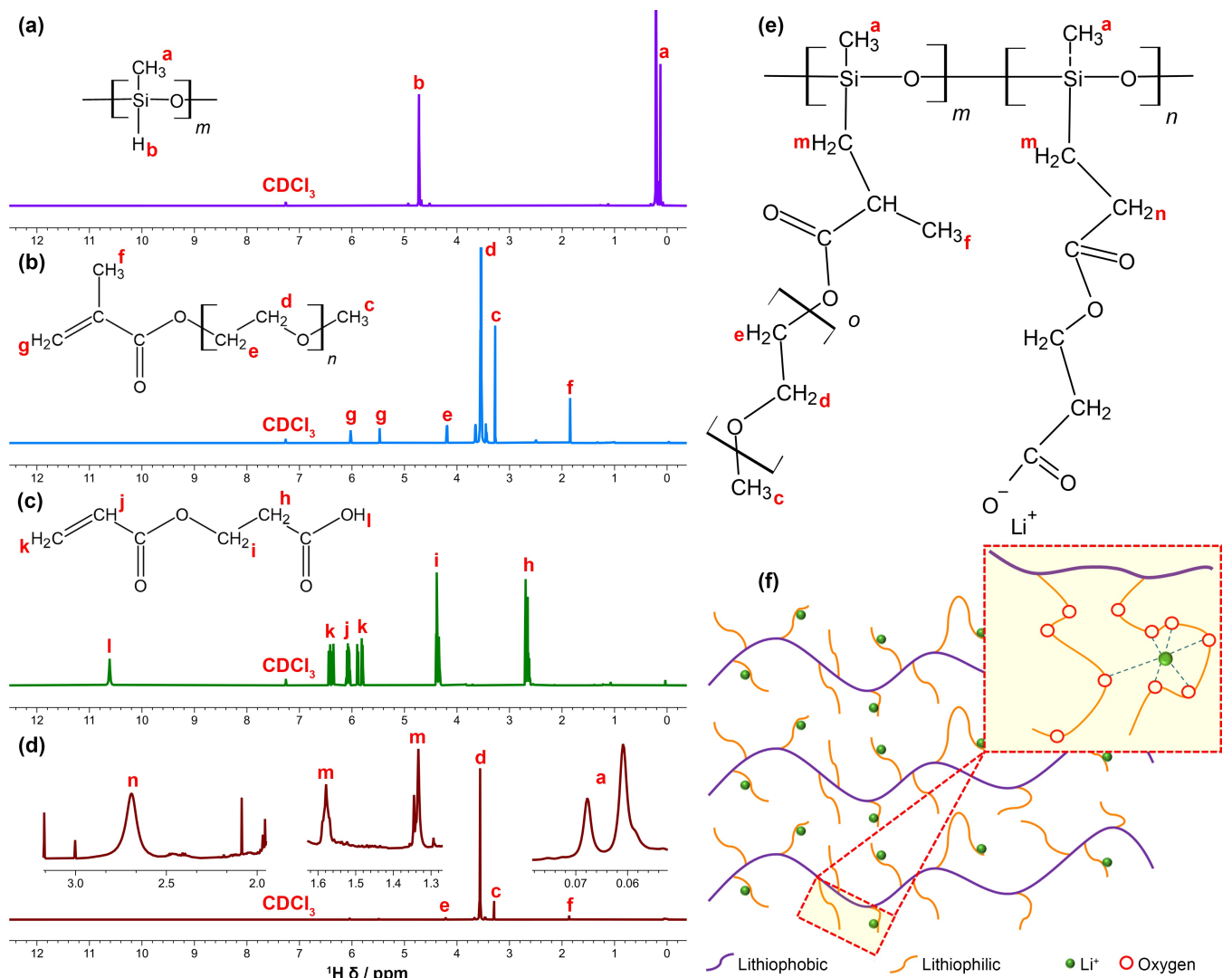


Figure 1. ¹H-NMR of (a) PMHS, (b) PEGMEMA, (c) CEA, (d) synthesized PE. (e) Chemical structure of PE and (f) its physical appearance illustration.

as shown in Figure 1b. The ethylene oxide chains of PEGMEMA are indicated in peak "d" and "e". The presence of methyl methacrylate isomer is shown in peak "f" and peak "g". Meanwhile, peak "c" indicates the methyl group at the edge of the polymer. In the $^1\text{H-NMR}$ of CEA (Figure 1c), the δ (ppm) at 10.61 (peak "l"), 5.81–6.38 (peak "j" and "k"), 4.39 (peak "i"), and 2.69 (peak "h") correspond to the OH bond, C=C bond, and C–C bond (peak "i" and "h"), respectively. Based on the $^1\text{H-NMR}$ spectra, all the precursors have no defect. The PE was successfully synthesized through the hydrosilylation reaction which is catalyzed by Pt ion. This is indicated by the removal of Si–H bond as observed in the disappearance of peak "b" at 0.47 ppm in Figure 1d. In which followed by the disappearance of C=C bonds of CEA and PEGMEMA as indicated by the disappearance of peak "j" and "k" in $^1\text{H-NMR}$ as well as the removal of peak at a wavenumber of 1634 cm^{-1} in FTIR spectra of PE (Figure 1d and Figure S1). In addition, $^1\text{H-NMR}$ at δ (ppm) of 1.3–1.6 (peak "m") and 2.7 (peak "n") appeared in synthesized PE as an indicator of hydrosilylation reaction completion (Figure 1d). The removal of OH bond of CEA (peak "l" at 10.61 ppm) in PE structure indicates the successful proton exchange between H^+ and Li^+ . The chemical structure of PE is then drawn in Figure 1e. The lithiophilic side (ethylene oxide side chains) and the lithiophobic side (PMHS backbone) of the PE provide unique routes for lithium-ion transport (Figure 1f).^[28] This lithiophilic side assists the migration and hopping of Li^+ from one coordination site to another through segmental motion (inset Figure 1f).^[29]

Afterwards, PE was coated on bare Cu current collector as shown in Figure 2a. This preparation is explained in the experimental method. The surface morphology of the current collector is displayed in Figure 2b–e. The bare Cu has inhomogeneous surface morphology (Figure 2b and d). After the PE coating, the black spot and the lower image's contrast were observed (Figure 2c). The black spot in PE@Cu is likely due to the thicker polymer layer which is caused by the inhomogeneity of the bare Cu surface. Meanwhile, the lower SEM image's contrast of PE@Cu is due to the lower secondary electron emission of polymer than metal. In average, the PE layer on bare Cu is 3 μm thick as calculated from the cross-sectional SEM image (Figure 2e).

An initial galvanostatic plating-stripping test of half-cell configuration was conducted by using Aurbach method (Figure 3a and b).^[30,31] First, 1 mAh cm^{-2} lithium is plated at 0.05 mA cm^{-2} current density (Figure 3c). Afterwards, 0.5 mAh cm^{-2} lithium is stripped and plated continuously at 0.1 mA cm^{-2} until a total 10 cycle is achieved. At last, lithium is stripped until 1 V at 0.05 mA cm^{-2} current density (Figure 3d). The areal capacity of 0.86 mAh cm^{-2} and 0.91 mAh cm^{-2} are obtained from bare Cu and PE@Cu, respectively. PE@Cu generated a 5% higher reversible capacity than bare Cu. The overpotential, the difference of the voltage dip and the beginning of electrochemical deposition, of both current collectors are observed in Figure 3c. The overpotential in the initial plating is due to the overcoming of the nucleation barrier during lithium nucleation site formation on the Cu foil.^[32] Based on the phase diagram from Yan *et al.*, lithium cannot form a

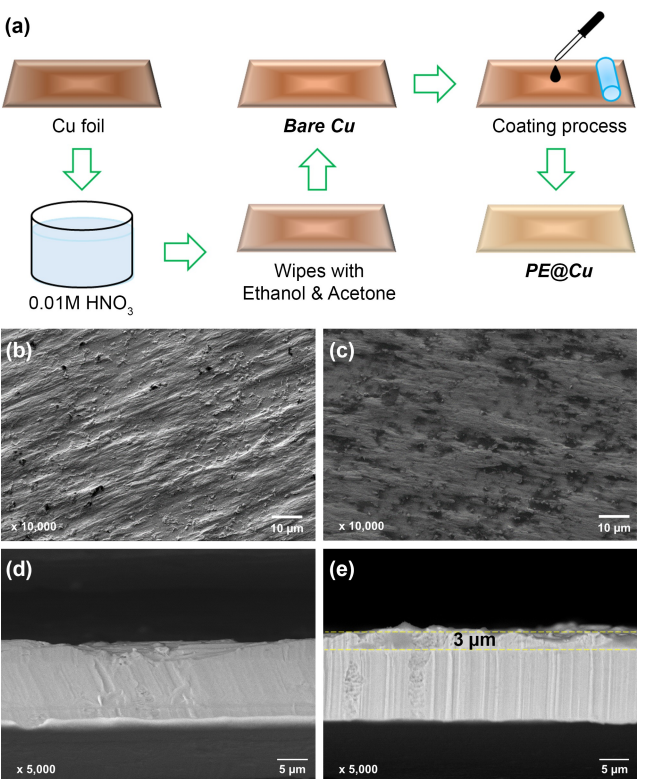


Figure 2. (a) Schematic preparation of Bare Cu and PE@Cu current collectors. Top view SEM images of (b) bare Cu and (c) PE@Cu. Cross-sectional SEM images of (d) bare Cu and (e) PE@Cu.

solid solution with Cu.^[33] Thus, it causes a large thermodynamic mismatch between lithium and cooper; in which creates a nucleation barrier.^[17] According to reference,^[33] the overpotential of lithium plated on Cu is ~40 mV at the lithium plating current of 10 μA . Meanwhile, in this work the overpotential of bare Cu and PE@Cu is 48.2 mV and 44.4 mV, respectively. Considering a higher initial lithium plating current in this work (0.056 mA), the overpotential values are still comparable with reference.^[33] After PE is coated on bare Cu, the overpotential is reduced by 3.8 mV (Figure 3c). This slight reduction in overpotential is likely due to the readily available small amount of lithium in the PE structure (Figure 1e). In which contributes to the increasing of lithium affinity on the PE@Cu compared with the bare Cu. However, this small difference in overpotential between bare Cu and PE@Cu and their comparable overpotential value with the reference indicate that lithium is probably still in direct contact with the Cu during initial plating.^[33]

In other words, PE acts as a pathway which regulates the mass transport of the Li^+ flux (inset Figure 1f). After the nucleation process ($t > 2\text{ h}$), which is marked with the red dotted line in Figure 3c, potential rises as it enters the lithium growth region.^[17] In this region, as time proceeds, bare Cu suffers from potential decay; it is pointed by the green arrow in Figure 3c. This behavior correlates with the lithium dendrite growth.^[34] Hence, the stable potential of PE@Cu in the same

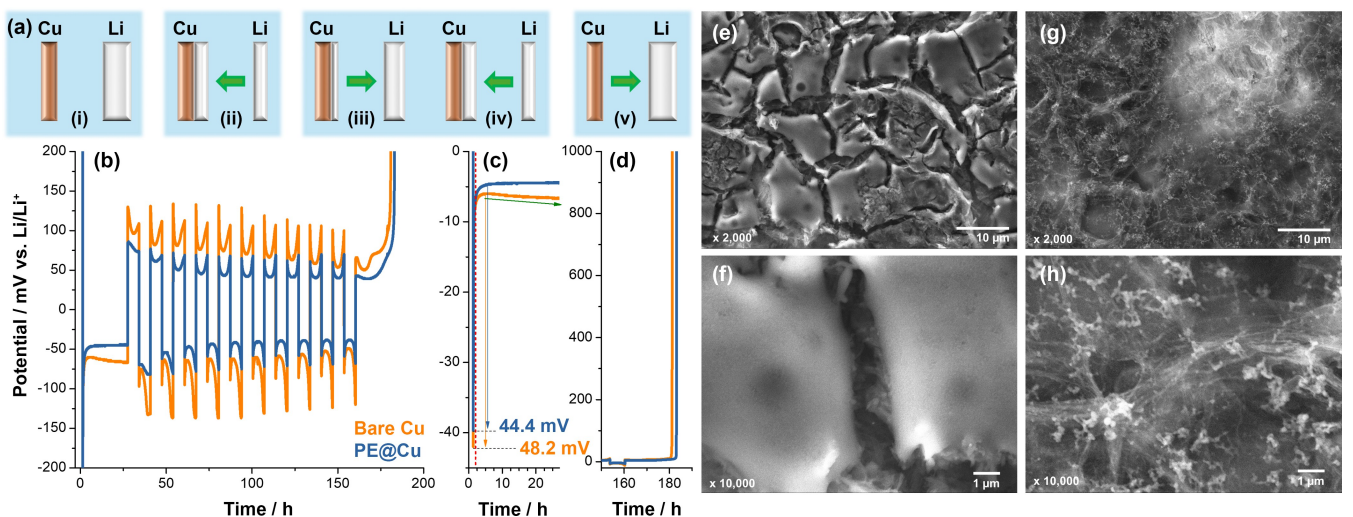


Figure 3. (a) Schematic illustration of Aurbach method (This image is adopted from the reference 28); (i) initial state of Cu || Li cell, (ii) lithium is deposited onto Cu with capacity of QT, (iii) fixed amount of Li stripped with capacity of QC (where QC < QT), (iv) fixed amount of Li deposited (QC), and (v) Li is exhaustively stripped. Aurbach profiles of Li/Cu cells using bare Cu (orange) and PE@Cu (blue); (b) Full profiles plot, (c) initial Li deposition, and (d) last lithium stripping to 1 V profiles. SEM images of harvested (e, f) bare Cu and (g, h) PE@Cu after Aurbach method Li/Cu cell cycle test.

region means that PE@Cu regulates the lithium dendrite growth at the initial lithium plating.

In the continuous stripping-plating test (Figure 3b), bare Cu suffers from a larger potential polarization than PE@Cu. Since the cycling test was performed at half of the initial lithium deposition capacity, the cycling test is affected by the initial solid electrolyte interphase (SEI) layer formation. The SEI layer builds resistance which causes potential polarization. Thus, larger potential polarization points to a thicker SEI layer on bare Cu. The formation of thick SEI layer on bare Cu is originally induced by the potential decay phenomena in the initial lithium plating (Figure 3c). Based on the lithium deposition observation of Huang *et al.* by using optical microscopy,^[32] in the continuous plating condition, the next lithium plated on Cu is likely to grow on the granular lithium which emerged from the nucleation site of the initial lithium plating. Therefore, this induces a thickening of the SEI layer in the subsequent plating.

Meanwhile, a sharp increase in potential at the end of stripping process is attributed to the formation of dead lithium on the bare Cu.^[32] Thus, overall, higher potential polarization of stripping-plating processes not only indicates the formation of SEI but also dead lithium formation. In contrast, PE@Cu has a lower potential polarization as an indicator of thinner SEI layer and less dead lithium on PE@Cu. Hence, PE@Cu has larger reversible capacity at the complete stripping process (Figure 3d).

At the end of the testing, both cells were dismantled in the argon filled glovebox. The harvested bare Cu and PE@Cu were washed in dimethyl carbonate (DMC) and dried at room temperature overnight. The SEM images of both harvested current collectors are displayed in Figure 3e–h. After cycles, large dense particles of ~10 μm width were observed on the bare Cu with an observable gap separated from each particle (Figure 3e and f). This gap in between these large particles indicates the nonuniformity of the lithium growth on the bare

Cu which left some blank areas. This large dense particle is likely attributed to the dead lithium; in which causes a higher irreversible capacity of 14% in bare Cu. Interestingly, after the total stripping process, a fibrous layer with nano-sized particles was observed on PE@Cu (Figure 3g and h). The fibrous like is probably from the lithiated PE which morphology is similar to the illustration in Figure 1f. Meanwhile, the nano-sized particles are likely attributed to the irreversible inactive lithium. This inactive lithium in the PE structure is likely due to the carbonyl functional groups are activated during the redox reaction to consume the lithium.^[35] In conclusion, the additional PE layer on bare Cu tailors the lithium deposition on Cu through its unique lithophilic and lithiophobic side chains which influences the cycle behavior (Figure 1f).

The X-ray photoelectron spectroscopy (XPS) was performed to further understand the inactive lithium, chemical composition, and SEI of both harvested current collectors (Figure 4). Figure 4a and b show the O 1s XPS spectra of bare Cu and PE@Cu. The peak at ~528.9 eV, ~530.5 eV, and ~531.5 eV is associated with Li₂O, Li₂O₂, and C=O, respectively.^[7,36] After cycle, Li₂O was observed only on bare Cu. This likely attributed to the inactive lithium formation after the reduction of Cu oxides (e.g., Cu₂O + 2Li⁺ + 2e⁻ → 2Cu + Li₂O).^[37] Meanwhile, Li₂O₂ can be found as an intermediate Cu oxide reduction reactions.^[38,39] However, Menkin *et al.* mentioned that Li₂O₂ could be a product of the reaction between high-surface-area Li microstructures with the oxygen in the glovebox or during the transfer to the XPS chamber.^[7] After exhaustive stripping process, PE@Cu has lower amount of this compound at ~530.5 eV than bare Cu. This suggests that PE@Cu has lower amount of inactive lithium. This in agreement with the Li 1s XPS spectra where the overall intensity of this peak on PE@Cu is lower than bare Cu (Figure 4c and d). The peak at ~531.5 eV can be assigned to the decomposition products of carbonate solvent (Figure 4a and b).^[40] However, in the case of PE@Cu this

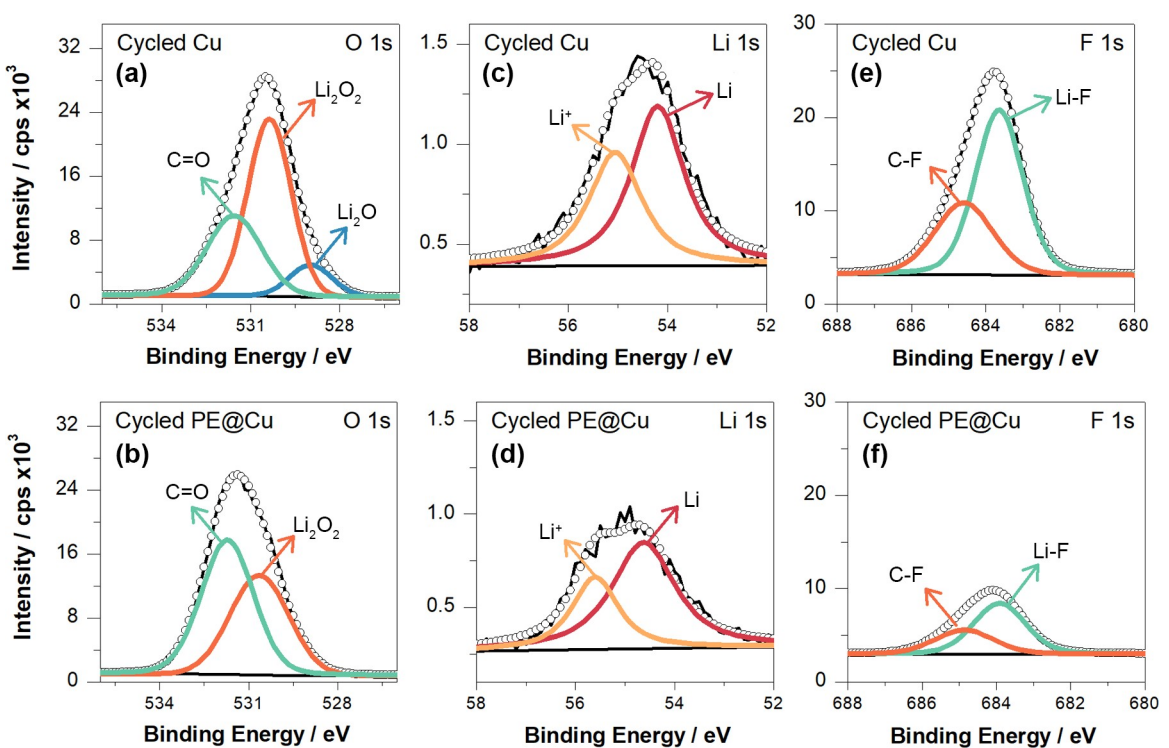


Figure 4. (a–b) O 1s, (c–d) Li 1s, and (e–f) F 1s XPS spectra of harvested (top row) bare Cu and (bottom row) PE@Cu after the Aurbach testing method as shown in Figure 3a–d.

peak also can be assigned to the PE as its structure consists of carbonyl functional group. Thus, higher intensity of peak at ~531.5 eV on PE@Cu cannot be directly addressed to the severe carbonate solvent decomposition than bare Cu. The salt decomposition can be observed in the F 1s XPS spectra (Figure 4e and f). The two peaks at ~683.7 eV and ~684.8 eV is assigned to Li–F and C–F, respectively.^[41] The fluorinated compounds formed due to the salt decomposition which in this work relates to the reductive reaction of LiDFOB.^[41,42] Hence, compared to bare Cu, PE@Cu possessed significantly lower electrolyte's salt decomposition byproducts. This proves that PE coated on Cu substrate reduces the parasitic side reaction with the electrolyte during the electrochemical performance test.

The uniformity of lithium deposition at the early stage of nucleation and growth of lithium was further observed at different current densities of 0.5 mA cm^{-2} and 5.0 mA cm^{-2} (Figure 5 and Figure 6). The lithium plating overpotential of bare Cu and PE@Cu at current densities of 0.5 mA cm^{-2} and 5.0 mA cm^{-2} are comparatively similar (Figure 5a and b). However, after the addition of PE on bare Cu, the initial voltage plateau shifts to lower capacity. This plateau is attributed to conversion reactions of surface oxides.^[37] This consistent with the presence of Li_2O in the O 1s XPS spectra of bare Cu (Figure 4a). As the surface oxides in Cu foil are considered a defect, this conversion reaction causes a nonuniformity lithium deposition. Interestingly, PE on bare Cu reduces this conversion reaction. In combination with the ability to tailor the lithium deposition, the PE@Cu has better uniformity of lithium plating on the surface (Figure 6). In the current density of 0.5 mA cm^{-2} ,

both current collectors show a micron-sized whisker like morphology of deposited lithium as seen in Figure 6a and b. But more Cu surface was covered by lithium on PE@Cu than on bare Cu. As the current density increases tenfold, the deposited lithium decreases in size, and it is more densely packed. This observation agrees with the investigation that has previously been done in references.^[17,43] Compared with bare Cu, the deposited lithium on the PE@Cu is smaller in size, more uniform, and more closely packed; no Cu surface can be observed (Figure 6b). The distributed lithiophilic chains in the lithiophobic chains of PE prevents the heterogeneous Li nucleation. Thus, it promotes a more uniform lithium deposition compared to bare Cu. This uniformity reduces the uneven Li^+ aggregation on the current collector during the prolonged cycle.^[44]

The 140 hours plating-stripping test was conducted at current density of 0.5 mA cm^{-2} in a cut-off capacity of 0.5 mAh cm^{-2} (Figure 7a and b). Thick Li metal of $300 \mu\text{m}$ as a counter electrode compensates for the lithium loss in each cycle. When compared with the bare Cu which suffers from fluctuations and high potential polarization, the PE@Cu current collector showed a significantly stable potential during ~140 hours plating-stripping tests (Figure 7b). A repeatable trend in shorter period of plating-stripping tests were obtained as shown in Figure S2a–d. On the selected cycle (Figure 7c and d), the stripping overpotential of bare Cu and PE@Cu is 32.4 mV and 1.5 mV, respectively. A huge difference in this stripping overpotential further proves that PE@Cu positively affects the lithium cation transport on the Cu surface as well as reduces

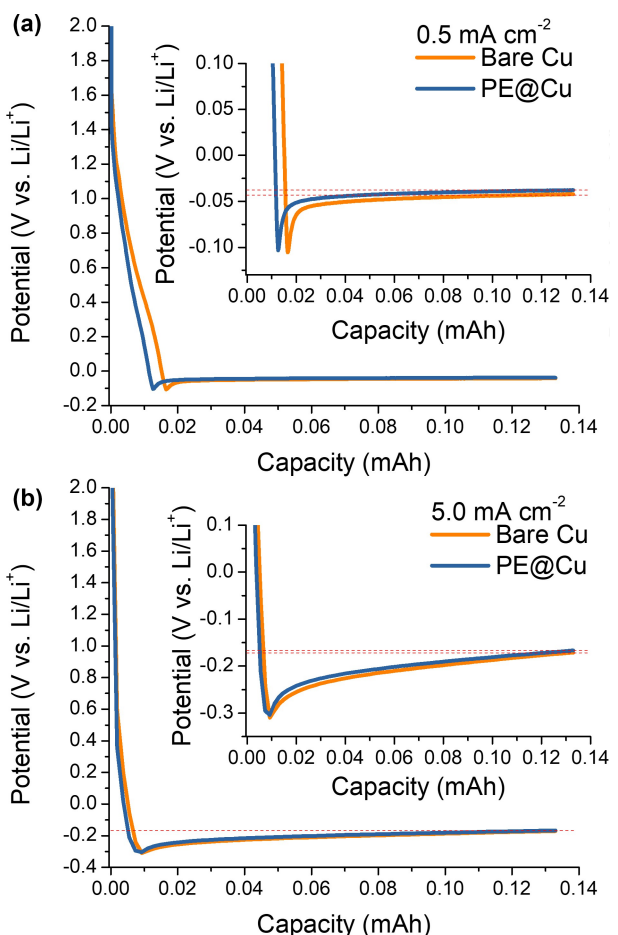


Figure 5. The voltage profile of 0.1 mAh cm^{-2} Li deposited on bare Cu (orange) and PE@Cu (blue) at current density of (a) 0.5 mA cm^{-2} and (b) 5.0 mA cm^{-2} .

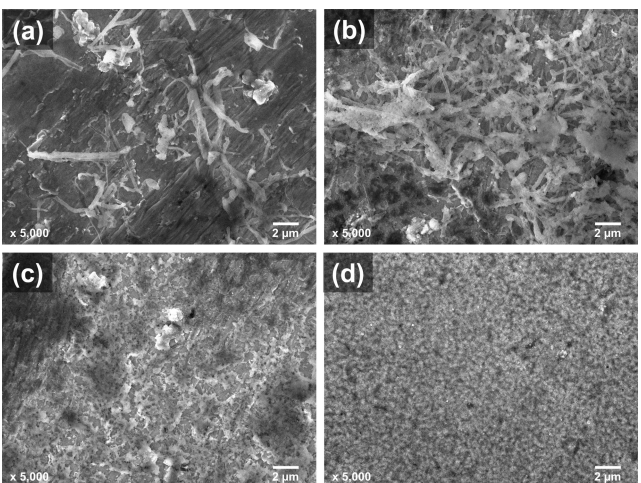


Figure 6. SEM images of 0.1 mAh cm^{-2} Li deposited on (a, c) bare Cu and (b, d) PE@Cu at current density of (a, b) 0.5 mA cm^{-2} and (c, d) 5.0 mA cm^{-2} .

the parasitic side reaction.^[45] After 15 plating-stripping cycles (Figure S2a-d), both cells were disassembled. A cleaner Cu and Li surfaces were observed in the cell with PE@Cu as a current collector (Figure S2e-f). An uneven dead lithium and cracked

SEI layer were observed on the bare Cu compared to PE@Cu (Figure S2g-h). As a result, cell with bare Cu suffers from a large impedance evolution than cell with PE@Cu as current collector (Figure S3). Thus, it inhibits lithium migration in a prolonged cycle on cell with bare Cu as a current collector. All these findings suggest that PE may also act as an ion selective membrane.^[45]

Finally, a full cell test is demonstrated with layered Ni-rich oxide cathode ($\text{LiNi}_{0.83}\text{Co}_{0.12}\text{Mn}_{0.015}\text{O}_2$, NCM83) (Figure 7e). At 50th cycle, bare-Cu || NCM83 and PE@Cu || NCM83 exhibit discharge capacity (capacity retention) of 48.1 mAh g^{-1} (23.8%) and 123.5 mAh g^{-1} (63.9%), respectively. In addition, the average coulombic efficiency of PE@Cu || NCM83 (98.1%) is 1.4% higher than bare-Cu || NCM83 (96.7%). This is contributed to the less inactive lithium in PE@Cu than bare Cu. Thus, the full cell with PE@Cu anode shows a significantly better cycle stability than with bare Cu anode.

Conclusions

In summary, the functionalized polysiloxane (PE) was successfully synthesized through Pt catalyzed hydrosilylation reaction. The arrangement of lithophilic and lithiophobic side chains of PE provides unique routes of Li^+ migration which tailors the lithium deposition on Cu current collector. This tailored initial lithium deposition induces lower plating-stripping potential polarizations, higher reversibility (5% higher than bare Cu), and improves the cycle stability of the full-cell configuration. In combination with NCM83, full-cell with PE@Cu anode improves the cycle stability by ~40% versus bare Cu as an anode. These findings are expected to give an additional understanding on the lithium deposition pathway which appears to be applicable for the development of high energy density lithium-ion batteries.

Experimental Method

Synthesis of Functionalized Polysiloxane (PE)

The synthesis method was adopted from the reference.^[25,27] 0.99 gram Poly(methylhydrosiloxane) (PMHS, $M_w = 1700\text{--}3200$, Sigma Aldrich), 12.825 gram poly(ethyl glycol) methyl ether methacrylate (PEGMEA, $M_n = 950$, Sigma-Aldrich), 0.216 gram 2-carboxyethyl acrylate (CEA, Sigma-Aldrich), and 10 μL Pt catalyst (Platinum(0)-1,3-divinyl-1,1,3,3-tetramethyldisiloxane, soln. in vinyl terminated polydimethylsiloxane, Alfa Aesar) were mixed with 200 mL tetrahydrofuran (THF, Tedia). This mixture was slowly stirred at 80°C for 72 hours under continuous nitrogen flow in 250 mL three neck round flask (borosilicate, Duran). A colorless homogeneous solution was then obtained. Afterwards, 0.189 gram $\text{LiOH}\cdot\text{H}_2\text{O}$ (98%, Thermo Scientific) was added to the solution. Another 24 hours were added to this mixing process, while the temperature was maintained at 80°C . Finally, the resulting solution was washed with *n*-hexane to remove the catalyst and residual precursor. The final product was then vacuumed and transferred to glovebox.

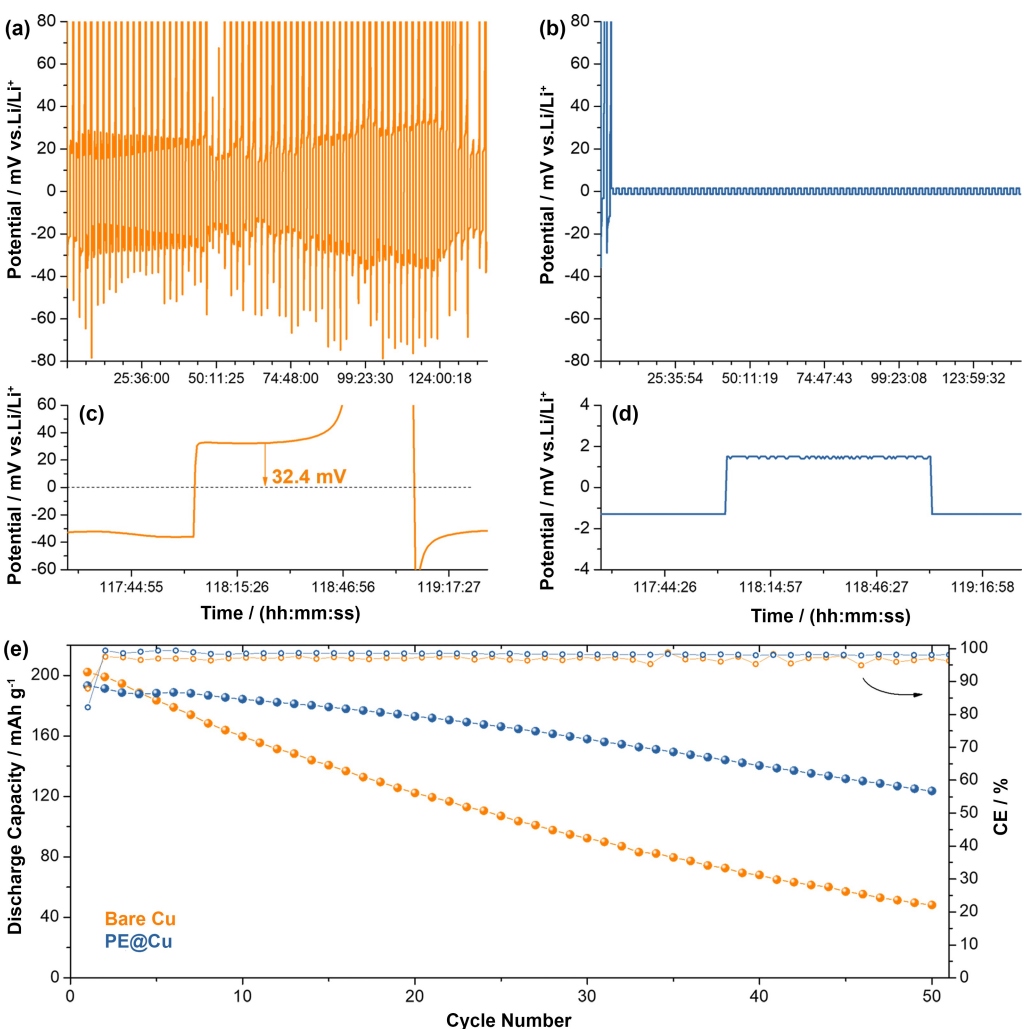


Figure 7. The voltage profile of 0.5 mAh cm^{-2} continuous Li plating/stripping on (a) bare Cu and (b) PE@Cu at current density of 0.5 mA cm^{-2} . Selected voltage profile of Li stripping at cycle 60th of (c) bare Cu and (d) PE@Cu from figure 6a and b, respectively. (e) Cycle stability test of bare-Cu | NCM83 (orange) and PE@Cu | NCM83 (blue) full cells.

Current Collector Preparation

The schematic preparation of both current collectors is shown in Figure 2a. Bare Cu foil was obtained after washing the Cu foil in 0.01 M HNO_3 , then subsequently wiped with ethanol and acetone to remove any water. The Bare Cu foil was then vacuumed at 60°C for 12 h prior to moving into glovebox. The freshly prepared PE was then coated on the Bare Cu foil with doctor blade above the hotplate at 60°C inside Argon filled glovebox. The PE coated bare Cu foil was then dried overnight at room temperature to obtain the PE@Cu. Both current collectors (Bare Cu and PE@Cu) are cut in circles with 13 mm diameter.

$\text{LiNi}_{0.83}\text{Co}_{0.12}\text{Mn}_{0.05}\text{O}_2$ (NCM83) Electrode Preparation

The NCM83 cathode powder was purchased from UBIQ Technology Co, Ltd., Taiwan. The NCM83 cathode was kept in Argon filled glovebox at oxygen and water content less than 0.5 ppm as received. The cathode was prepared by mixing 90% NCM83 powder, 5% Super-P (Timcal), and 5% PVDF binder (Solef 5130, Solvay) in *n*-Methyl-2-pyrrolidone (NMP, UBIQ Technology Co, Ltd.) with solid to liquid weight ratio of 4:6. This mixture was vigorously mixed at 1400 rpm for 2 hours with mechanical stirrer to form

homogenous slurry. The homogenous slurry was then casted with $100 \mu\text{m}$ doctor blade on an Aluminum current collector and dried in a convection oven at 70°C for 30 mins. After calendared to remove 30% thickness and cut in circle at 12 mm diameter, the cathode was dried overnight in vacuum at 120°C prior to moving into glovebox. The active mass areal loading of the cathode is $\sim 4.5 \text{ mg cm}^{-2}$.

Material Characterization

Proton Nuclear Magnetic Resonance ($^1\text{H-NMR}$; Bruker Avance III HD-600 MHz NMR) is performed to confirm the structure of precursors and PE using chloroform-*d* (CDCl_3) as the solvent. The sample to solvent ratio for $^1\text{H-NMR}$ is controlled at weight ratio of 1:10. The Fourier Transform Infrared Spectroscopy with Attenuated Total Reflection add-on (FTIR-ATR; JASCO 6700) is conducted to understand the structure of precursors and final synthesized products. To prevent interference from the ambient atmosphere, FTIR-ATR was operated under the nitrogen filled glovebox. All morphologies are captured by using JEOL JSM-7600F scanning electron microscopy (SEM) at an operating voltage of 10 kV.

Electrochemical Performance Test

2032-type coin cell was used for all the electrochemical performance test, as well as 20- μm -thick Celgard® 2320 tri layer PP/PE/PP separator and 20 μL 1 M LiDFOB in a mixture of ethylene carbonate (EC) and dimethyl carbonate (DMC) with volume ratio of 3:7 as an electrolyte. The half-cell configuration tests (bare-Cu||Li and PE@Cu||Li) were conducted using bare Cu and PE@Cu current collectors with Li metal (300 μm thick from UBIQ Technology Co., Ltd.) as the counter electrode. The galvanostatic cycling tests were carried out at 30 °C using battery tester equipment from Neware. The full cell configurations (bare-Cu||NCM83 and PE@Cu||NCM83) were tested in a potential window range of 2.5–4.3 V with 2 formation cycles at 0.1 C and at 0.2 C for the following cycles. 1 C current rate corresponded to 200 mA g^{-1} current density.

Author Contributions

R.A. Yuwono: Writing-original draft, Methodology, Investigation, Formal Analysis, Validation, Data Curation, Visualization, Writing-review & editing. P.X. Yu: Methodology, Data Curation. R. Foeng: Methodology, Data Curation. C. Khotimah: Investigation, Formal Analysis, Methodology, Data Curation, Writing-review & editing. S. Salshabilla: Methodology, Data Curation. F.M. Wang: Writing-review & editing, Conceptualization, Supervision, Funding acquisition, Project administration, Resources. M.T. Tang: Funding acquisition. N. L. Wu: Resources.

Acknowledgements

Prof. F.M. Wang is grateful for the financial support from the National Science and Technology Council (NSTC) and the Ministry of Education (MOE, "Sustainable Electrochemical Energy Development Center" (SEED)) project of Taiwan, R.O.C., under grant numbers 110-2923-E-007-005, 111-2622-E-01-013-, 111-3116-F-011-005-, 112-2923-E-007-005, 112-2622-E-01-026, and 112-2221-E-011-013-MY3. Prof. N. L. Wu thanks the financial support of the "Advanced Research Center for Green Materials Science and Technology" (Ministry of Education (TW), project number: 112L9006) and of the National Science and Technology Council (TW) under contract number of NSTC-110-2221-E-002-015-MY3 and 112-2923-E-011-005. The Author also acknowledges Mrs. Su-Jen Ji from Instrument Center, College of Science, National Taiwan University for aiding in SEM measurements and Ms. Yi-Jin Wei from Center for Plasma and Thin Film Technologies, Ming Chi University of Technology for aiding in XPS measurements.

Conflict of Interests

The authors declare no conflict of interest.

Data Availability Statement

The data that support the findings of this study are available from the corresponding author upon reasonable request.

Keywords: Lithium metal • Functionalized polysiloxane • Lithiophilic coating • Lithium deposition • Ni-rich cathode

- [1] H. Wang, K. Feng, P. Wang, Y. Yang, L. Sun, F. Yang, W.-Q. Chen, Y. Zhang, J. Li, *Nat. Commun.* **2023**, *14*, 1246.
- [2] International Energy Agency, "Trends in charging infrastructure", can be found under <https://www.iea.org/reports/global-ev-outlook-2023-trends-in-charging-infrastructure>, 2023 (accessed 5 July 2024).
- [3] C. Niu, D. Liu, J. A. Lochala, C. S. Anderson, X. Cao, M. E. Gross, W. Xu, J.-G. Zhang, M. S. Whittingham, J. Xiao, J. Liu, *Nat. Energy* **2021**, *6*, 723.
- [4] B. Wu, Y. Yang, D. Liu, C. Niu, M. Gross, L. Seymour, H. Lee, P. M. L. Le, T. D. Vo, Z. D. Deng, E. J. Dufek, M. S. Whittingham, J. Liu, J. Xiao, *J. Electrochem. Soc.* **2019**, *166*, A4141.
- [5] R. Schmuck, R. Wagner, G. Hörpel, T. Placke, M. Winter, *Nat. Energy* **2018**, *3*, 267.
- [6] A. J. Louli, M. Genovese, R. Weber, S. G. Hames, E. R. Logan, J. R. Dahn, *J. Electrochem. Soc.* **2019**, *166*, A1291.
- [7] S. Menkin, C. A. O'Keefe, A. B. Gunnarsdóttir, S. Dey, F. M. Pesci, Z. Shen, A. Aguadero, C. P. Grey, *J. Phys. Chem. C* **2021**, *125*, 16719.
- [8] D. Lin, Y. Liu, Y. Cui, *Nat. Nanotech.* **2017**, *12*, 194.
- [9] C. Yang, K. Fu, Y. Zhang, E. Hitz, L. Hu, *Adv. Mater.* **2017**, *29*, 1701169.
- [10] Y.-T. Weng, H.-W. Liu, A. Pei, F. Shi, H. Wang, C.-Y. Lin, S.-S. Huang, L.-Y. Su, J.-P. Hsu, C.-C. Fang, Y. Cui, N.-L. Wu, *Nat. Commun.* **2019**, *10*, 5824.
- [11] J. Luo, C. Fang, N. Wu, *Adv. Energy Mater.* **2018**, *8*, 1701482.
- [12] K. B. Hatzell, *ACS Energy Lett.* **2023**, *8*, 4775.
- [13] H. Zhong, Y. Zhao, T. Zhang, G. Liu, *Batteries Supercaps* **2021**, *4*, 98.
- [14] S. Stuckenbergs, M. M. Bela, C. Lechtenfeld, M. Mense, V. Küpers, T. T. K. Ingber, M. Winter, M. C. Stan, *Small* **2024**, *20*, 2305203.
- [15] P. Afzali, E. Gibertini, L. Magagnini, *Electrochim. Acta* **2024**, *488*, 144190.
- [16] C. Heubner, S. Maletti, O. Lohrberg, T. Lein, T. Liebmann, A. Nickol, M. Schneider, A. Michaelis, *Batteries Supercaps* **2021**, *4*, 1310.
- [17] A. Pei, G. Zheng, F. Shi, Y. Li, Y. Cui, *Nano Lett.* **2017**, *17*, 1132.
- [18] R. Weber, M. Genovese, A. J. Louli, S. Hames, C. Martin, I. G. Hill, J. R. Dahn, *Nat. Energy* **2019**, *4*, 683.
- [19] Y. Liang, W. Wu, D. Li, H. Wu, C. Gao, Z. Chen, L. Ci, J. Zhang, *Adv. Energy Mater.* **2022**, *12*, 2202493.
- [20] L. Suo, Y.-S. Hu, H. Li, M. Armand, L. Chen, *Nat. Commun.* **2013**, *4*, 1481.
- [21] X. Fan, C. Wang, *Chem. Soc. Rev.* **2021**, *50*, 10486.
- [22] F. Joho, P. Novák, *Electrochim. Acta* **2000**, *45*, 3589.
- [23] H. Duan, M. Fan, W. Chen, J. Li, P. Wang, W. Wang, J. Shi, Y. Yin, L. Wan, Y. Guo, *Adv. Mater.* **2019**, *31*, 1807789.
- [24] F.-M. Wang, Y.-Y. Wang, C.-C. Wan, *ECS Trans.* **2009**, *16*, 91.
- [25] F.-M. Wang, C.-C. Wan, Y.-Y. Wang, *J. Appl. Electrochem.* **2009**, *39*, 253.
- [26] F.-M. Wang, C.-C. Hu, S.-C. Lo, Y.-Y. Wang, C.-C. Wan, *J. Electroanal. Chem.* **2010**, *644*, 25.
- [27] K.-W. Liu, P.-H. Hsu, J.-K. Chang, F.-M. Wang, W.-R. Liu, *Ceram. Int.* **2024**, DOI: 10.1016/j.ceramint.2024.10.372.
- [28] R. Hooper, L. J. Lyons, M. K. Mapes, D. Schumacher, D. A. Moline, R. West, *Macromolecules* **2001**, *34*, 931.
- [29] Q. Zhao, S. Stalin, C.-Z. Zhao, L. A. Archer, *Nat. Rev. Mater.* **2020**, *5*, 229.
- [30] D. Aurbach, O. Youngman, Y. Gofer, A. Meitav, *Electrochim. Acta* **1990**, *35*, 625.
- [31] B. D. Adams, J. Zheng, X. Ren, W. Xu, J. Zhang, *Adv. Energy Mater.* **2018**, *8*, 1702097.
- [32] C.-J. Huang, B. Thirumalraj, H.-C. Tao, K. N. Shitaw, H. Sutiono, T. T. Hagos, T. T. Beyene, L.-M. Kuo, C.-C. Wang, S.-H. Wu, W.-N. Su, B. J. Hwang, *Nat. Commun.* **2021**, *12*, 1452.
- [33] K. Yan, Z. Lu, H.-W. Lee, F. Xiong, P.-C. Hsu, Y. Li, J. Zhao, S. Chu, Y. Cui, *Nat. Energy* **2016**, *1*, 16010.
- [34] K.-H. Chen, K. N. Wood, E. Kazyak, W. S. LePage, A. L. Davis, A. J. Sanchez, N. P. Dasgupta, *J. Mater. Chem. A* **2017**, *5*, 11671.
- [35] B. Atsbeha Kahsay, F.-M. Wang, A. G. Hailu, C.-H. Su, *Polymers (Basel)* **2020**, *12*, 1109.
- [36] D. Briggs, G. Beamson, *Anal. Chem.* **1993**, *65*, 1517.
- [37] Z. Zhang, X. Xu, S. Wang, Z. Peng, M. Liu, J. Zhou, C. Shen, D. Wang, *ACS Appl. Mater. Interfaces* **2016**, *8*, 26801.

- [38] A. B. Gunnarsdóttir, S. Vema, S. Menkin, L. E. Marbella, C. P. Grey, *J. Mater. Chem. A* **2020**, *8*, 14975.
- [39] X. Hua, R. Robert, L.-S. Du, K. M. Wiaderek, M. Leskes, K. W. Chapman, P. J. Chupas, C. P. Grey, *J. Phys. Chem. C* **2014**, *118*, 15169.
- [40] K. Kanamura, H. Tamura, Z. Takehara, *J. Electroanal. Chem.* **1992**, *333*, 127.
- [41] C.-Y. Liu, Y. Yang, M. Yao, H.-T. Fang, *Energy Storage Mater.* **2019**, *18*, 148.
- [42] M. Xu, L. Zhou, L. Hao, L. Xing, W. Li, B. L. Lucht, *J. Power Sources* **2011**, *196*, 6794.
- [43] J. Sun, J. Peng, T. Ring, L. Whittaker-Brooks, J. Zhu, D. Fragedakis, J. Niu, T. Gao, F. Wang, *Energy Environ. Sci.* **2022**, *15*, 5284.
- [44] Z. Wang, Z. Du, Y. Liu, C. E. Knapp, Y. Dai, J. Li, W. Zhang, R. Chen, F. Guo, W. Zong, X. Gao, J. Zhu, C. Wei, G. He, *eScience* **2024**, *4*, 100189.
- [45] Z. Li, L. Hou, X. Zhang, B. Li, J. Huang, C. Chen, Q. Liu, R. Xiang, Q. Zhang, *Battery Energy* **2022**, *1*, 20220006.

Manuscript received: July 15, 2024
Revised manuscript received: November 2, 2024
Accepted manuscript online: November 15, 2024
Version of record online: December 4, 2024
